Delft University of Technology

Intrinsic-Strain Engineering by Dislocation Imprint in Bulk Ferroelectrics

Zhuo, Fangping; Zhou, Xiandong; Gao, Shuang; Dietrich, Felix; Groszewicz, Pedro B.; Fulanović, Lovro; Breckner, Patrick; Xu, Bai Xiang; Kleebe, Hans Joachim; More Authors

Important note
To cite this publication, please use the final published version (if applicable).
Please check the document version above.

Intrinsic-Strain Engineering by Dislocation Imprint in Bulk Ferroelectrics

Fangping Zhuo [1,*,†] Xiandong Zhou [2,3,*] Shuang Gao,[1] Felix Dietrich,[4] Pedro B. Groszewicz,[5] Lovro Fulanović,[1] Patrick Breckner,[1] Bai-Xiang Xu,[1] Hans-Joachim Kleebe,[1] Dragan Damjanovic,[1,6] and Jürgen Rödel [1,‡]

[1]*Department of Materials and Earth Sciences, Technical University of Darmstadt, 64287 Darmstadt, Germany*
[2]*Failure Mechanics and Engineering Disaster Prevention Key Laboratory of Sichuan Province,*
College of Architecture and Environment, Sichuan University, Chengdu 610207, China
[3]*MOE Key Laboratory of Deep Earth Science and Engineering, College of Architecture and Environment,*
Sichuan University, Chengdu 610065, China
[4]*Institute of Physical Chemistry, Technical University of Darmstadt, 64287 Darmstadt, Germany*
[5]*Department of Radiation Science and Technology, Delft University of Technology, Delft 2629JB, Netherlands*
[6]*Institute of Materials, École Polytechnique Fédérale de Lausanne, 1015 Lausanne, Switzerland*

We report an intrinsic strain engineering, akin to thin filmlike approaches, via irreversible high-temperature plastic deformation of a tetragonal ferroelectric single-crystal $BaTiO_3$. Dislocations well-aligned along the [001] axis and associated strain fields in plane defined by the $[110]/[\bar{1}10]$ plane are introduced into the volume, thus nucleating only in-plane domain variants. By combining direct experimental observations and theoretical analyses, we reveal that domain instability and extrinsic degradation processes can both be mitigated during the aging and fatigue processes, and demonstrate that this requires careful strain tuning of the ratio of in-plane and out-of-plane domain variants. Our findings advance the understanding of structural defects that drive domain nucleation and instabilities in ferroic materials and are essential for mitigating device degradation.

As thin films adopt the eigenstrain of the substrate, they can be manipulated to exhibit large tensile or compressive in-plane strains [1–4]. For paraelectric $SrTiO_3$ this results in a transition to the ferroelectric state and a shift in Curie point by $\sim290\,°C$ [4]. For ferroelectric materials, this allows us to dramatically tune domain patterns and hence electromechanical properties [5–11], owing to their intrinsically strong couplings between lattice (strain) and charge (polarization) degrees of freedom (d.o.f.) [12,13]. For example, with a tensile (compressive) strain of $>1\%$, a domain population of 100% in-plane a_1/a_2 variants (out-of-plane c variants) was achieved in tetragonal ferroelectric films such as $BaTiO_3$ [6–9], $PbTiO_3$ [6,7,10], and $PbZr_{0.2}Ti_{0.8}O_3$ [11]. In particular, the application of reversible and biaxial elastic strains of several percent can enhance the remanent polarization by 250% and shift the Curie point by $\sim400\,°C$ in $BaTiO_3$ under a compressive strain of 1.7% [8], as compared to these values of the bulk. In relation to macroscopic biaxial strains, microscopic out-of-plane strains have also been achieved, leading to supertetragonal structures with a giant c/a (out-of-plane to in-plane lattice parameters) ratio of 1.238 [14]. Elastic strain engineering in thin films, however, so far lacks the ability to impose continuously tunable strain, unless an active substrate is used. Similar problems exist (with interphase strain in multiphase materials [14]) and defect-induced strain relaxation during growth [15,16], thereby hindering the strain

tuning of desired domain distribution and properties of ferroelectrics.

The applications of ferroelectrics are a consequence of their ability to nucleate domains and move domain walls (DWs) [17–19]. Perhaps less widely appreciated, irreversible and large local elastic strain fields can be imparted to bulk ferroelectrics through uniaxial plastic deformation [20–22], leading to permanent tailoring of the elastic energy of a given system. The bulk deformation is fundamentally different from strain engineering because it introduces extended one-dimensional lattice defects—dislocations—into the volume rather than at the interface [23]. Theoretical predictions have demonstrated that dislocations can serve as both the nucleation sites for new domains as well as the pinning centers for the motion of ferroelectric and ferroelastic DWs [24–26]. Such effects are drastically amplified in ferroelectric single crystals, when mesoscopic dislocations self-assemble into larger-scale structures such as arrays and networks. However, the concept of dislocation-tuned domain nucleation and domain stability has rarely been perceived as a microstructural tool to extend the local effects of dislocations to the macroscopic level of bulk ferroelectrics. This is because bulk oxides are inherently brittle and can only withstand a moderate compressive or tensile strain of $\sim0.1\%$, far below the level of accessible strains in thin films [27,28]. By overcoming this challenge using high-temperature

deformation [22,29], we recently revealed that imprinting dislocations into single-crystal BaTiO$_3$ favored c/a domain variants and yielded a 19-fold increase in piezo-electricity [22]. Despite the exciting functional harvesting in bulk ferroelectrics by dislocation imprint, however, the details of the mechanisms by which intrinsic dislocation-type lattice strains can control domain nucleation and domain stabilization, are still ambiguous.

In this Letter, we combine theoretical and experimental approaches to directly monitor domain nucleation and domain stability in a bulk ferroelectric by introducing dislocations into the volume. By recognizing the relation of accessible glide planes and DWs we identify useful interrelationships [Figs. 1(a) and 1(b)]. The crucial role of dislocation-induced lattice strains was considered by revisiting the in-plane planar tensile and compressive stress fields of two edge-type dislocations with a spacing of 50 nm. The computed local stresses responsible for lattice deformation can reach an order of GPa, which is comparable to the application of 1% lattice-mismatch strain for

FIG. 1. (a) Schematic showing the slip planes of the set of $\{100\}\langle100\rangle$ slip systems. The dislocations are characterized by dislocation line vector $\vec{\xi}$ (marked by red arrow) and Burgers vector $\vec{b}$, and typical 90° DWs are highlighted. In edge dislocations, the dislocation line vector and Burgers vector are perpendicular one another, namely, $\vec{\xi} \cdot \vec{b} = 0$. (b) Out-of-plane perfectly oriented dislocations can be extracted from (a). (c) The stress fields act as the nucleation sites for in-plane a_1-/a_2 domains in which dislocations with two mutually perpendicular Burgers vectors are parallel to the a_1/a_2 90° DWs. Note that the c domain has a polarization along the [001] direction, and a_1 and a_2 domains are defined by the in-plane polarizations along the [100] and [010] directions, respectively.

thin films (1–10 GPa of pressure) [30]. As a consequence of these particular dislocation orientations, only in-plane a_1/a_2-domain variants are spontaneously developed after reaching equilibrium when we set the initial random domain state, see phase-field simulation in Fig. 1(c), while the out-of-plane c domains vanish. Our simulations reveal that both negative and positive charges play a minor role when flipping down c domains (see Fig. S1 [31]). In contrast, if the dislocations are absent, a-/c domains naturally nucleate in the system, as displayed in Fig. S2 [31]. This suggests a new paradigm in which dislocation imprint will provide the guard rails for the formation of the domain structure. The dislocations can be transferred into self-organized structures that store their elastic energy spanning broad length scales (nm–mm).

For fundamental insights, a ferroelectric material is ideal, which allows us to imprint glide planes with a high density of aligned dislocations onto different crystallographic planes. This dislocation-type lattice strain field is best exposed in a tetragonal ferroelectric crystal with in-plane a_1-/a_2 variants and out-of-plane c variants [39,40], thus ensuring 90° and 180° DWs only. This is the case for single-crystal BaTiO$_3$, where at high temperatures two glide systems can be activated by loading along different directions [22,29,41]. Hence, dislocations can then be inserted both onto $\{100\}$ planes as well as on $\{110\}$ planes, offering different scenarios for monitoring domain nucleation and domain stability beyond the limits of the thin film-substrate interface.

As a didactic demonstration, we introduced perfectly oriented dislocation lines into BaTiO$_3$ *via* high-temperature plastic deformation by [110] loading, see the stress-strain curve in Fig. 2(a). Plastic deformation is mediated by the generation and motion of dislocations [42]. After deformation, macroscopic domain morphology was altered when compared with the undeformed reference sample [see inset in Fig. 2(a)]. Transmission electron microscopy (TEM) revealed the activation of the $\{100\}\langle100\rangle$ slip systems during uniaxial compression, see Fig. 2(b) and detailed analysis in Fig. S3 [31]. When we sliced the (001) plane from the deformed sample, the imprinted dislocations were well aligned in the out-of-plane [001] direction [Fig. 1(b)]. As expected, this dislocation arrangement dictates domain nucleation of only in-plane domains at the nanoscale, which was evidenced by TEM. As a non-destructive tool, nuclear magnetic resonance (NMR) spectroscopy offers the unique opportunity to quantify the domain distribution of BaTiO$_3$. The orientation of the electric field gradient (EFG) tensor at the barium site for a_1, a_2, and c domains, which determines the NMR frequency, is a direct function of the spontaneous polarization vectors [22,41,43]. NMR spectroscopy demonstrated that only in-plane domains are permissible in the entire deformed sample, whereas a large amount of c domains are present in the reference sample [Figs. 2(c) and 2(d)]. The favored
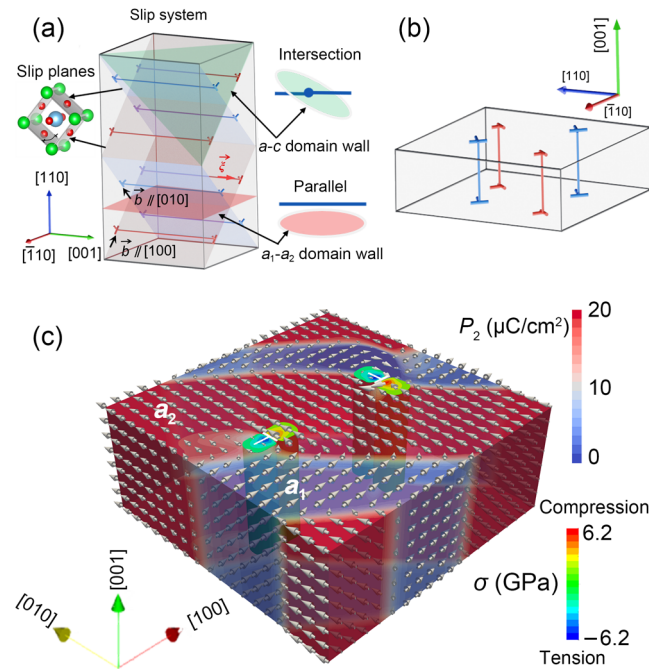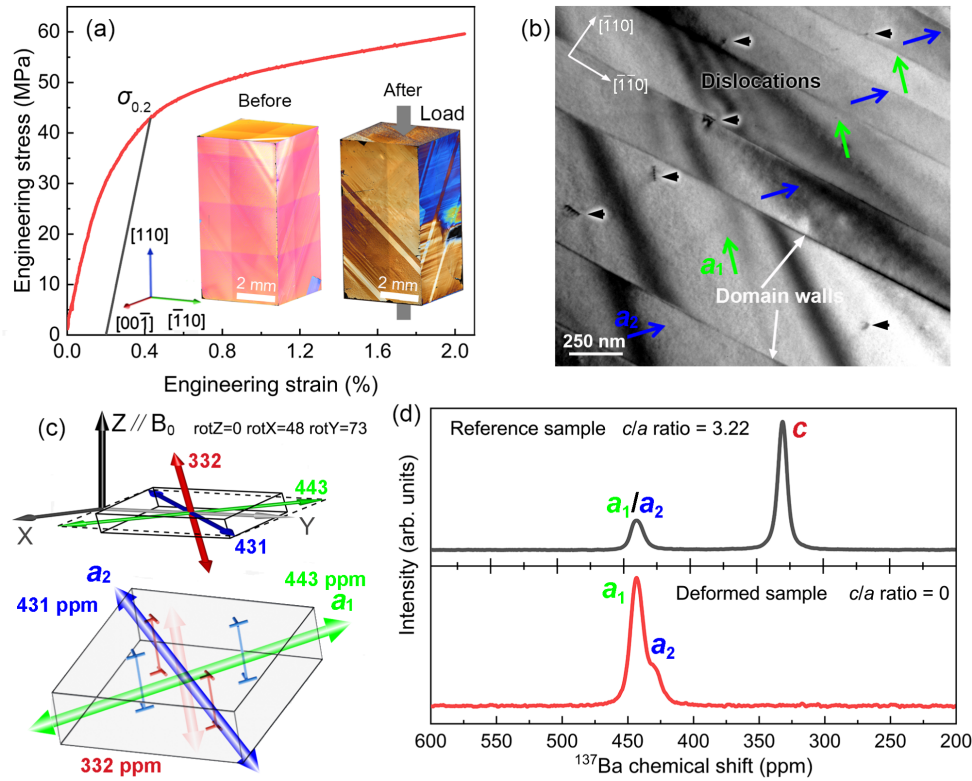
FIG. 2. (a) Uniaxial compression behavior of [110]-oriented $BaTiO_3$ single crystal obtained at 1150 °C by loading along the [110] direction. The yield strength (at 0.2% offset) is 43.6 MPa. The inset features the optical images of the reference and deformed samples. (b) TEM image taken along the [001] direction, confirming the nucleation of a_1 and a_2 domains on the (001) plane. The positions of dislocations and DWs are marked by black arrowheads and white arrows, respectively. (c) Schematic representing the orientations of the polarization vectors and dislocation arrangement. The rotation axis (y axis) is perpendicular to the magnetic field B_0 (z axis). For this specific set up of the goniometer NMR probe, the positions of the respective ^{137}Ba NMR signal for different domains can be detected at a given rotation angle of 20° (3° offset). An angle of 0° indicates the normal vector of the sample as parallel to the magnetic field B_0. (d) ^{137}Ba NMR spectra supporting the nucleation of the in-plane a_1 and a_2 domains in the entire deformed sample.

a_1/a_2 variants with 90° DWs were further verified by optical microscopy (Fig. S4 [31]). Interestingly, these a_1/a_2 90° DWs are curved rather than straight in the deformed sample, indicating macroscopic effects of dislocation-based strains on domain patterns. The a_1/a_2-domain structures were also analyzed by piezoresponse force microscopy (PFM, Fig. S5 [31]). By performing *in situ* observation using optical microscopy during heating and cooling (see video S1 and Fig. S6 [31]), we observed the nucleation of the herringbone patterns of needlelike a_1/a_2-domain structures. However, no similar features were documented in the reference sample (Fig. S7 [31]).

As featured in Fig. S8 [31], in our case of mechanical imprint, the Curie point of single-crystal $BaTiO_3$ was slightly increased due to the dislocation-induced strain fields (see our simulation in Fig. S9 [31] and Ref. [44]), and the dielectric permittivity (ε_{33}) was enhanced over the measured temperature range. As compared to the reference sample, macroscopic measurement on the polarization hysteresis loop revealed a fourfold increase in the coercive field ($E_c = 4.1$ kV/cm) and a reduced spontaneous polarization in the deformed sample (Fig. S10 [31]), supporting

domain-wall pinning [22,45,46]. The reference sample has a high fraction of c domains (94%) after field excitation, while the ratio of electric-field-induced c domains in the deformed sample is 69%.

Having established the correlation between $\langle 100 \rangle$-type dislocation lattice strain and the domain nucleation, we now address a fundamental question of the extent to which the imprinted dislocations can tune domain stability and related properties. For this purpose, we performed both aging and fatigue experiments. Considering that a_1/a_2 90° DWs are rigid since there is no driving force to move them by applying a subcoercive field along the [001] direction [37], they can be switched to a/c 90° DWs by efficient electric poling ($E > E_c$). First, we examined the direct piezoelectric coefficient (d_{33}) and ε_{33} during the aging process. In the deformed sample, the d_{33} considerably decreased after [001] poling while the corresponding ε_{33} increased [see Fig. 3(a)]. In comparison, both properties stabilized during aging after [110] poling (Fig. S11 [31]). We note that these properties of the reference sample maintained stable. The changes of d_{33} and ε_{33} in the deformed sample are related to dislocation-induced
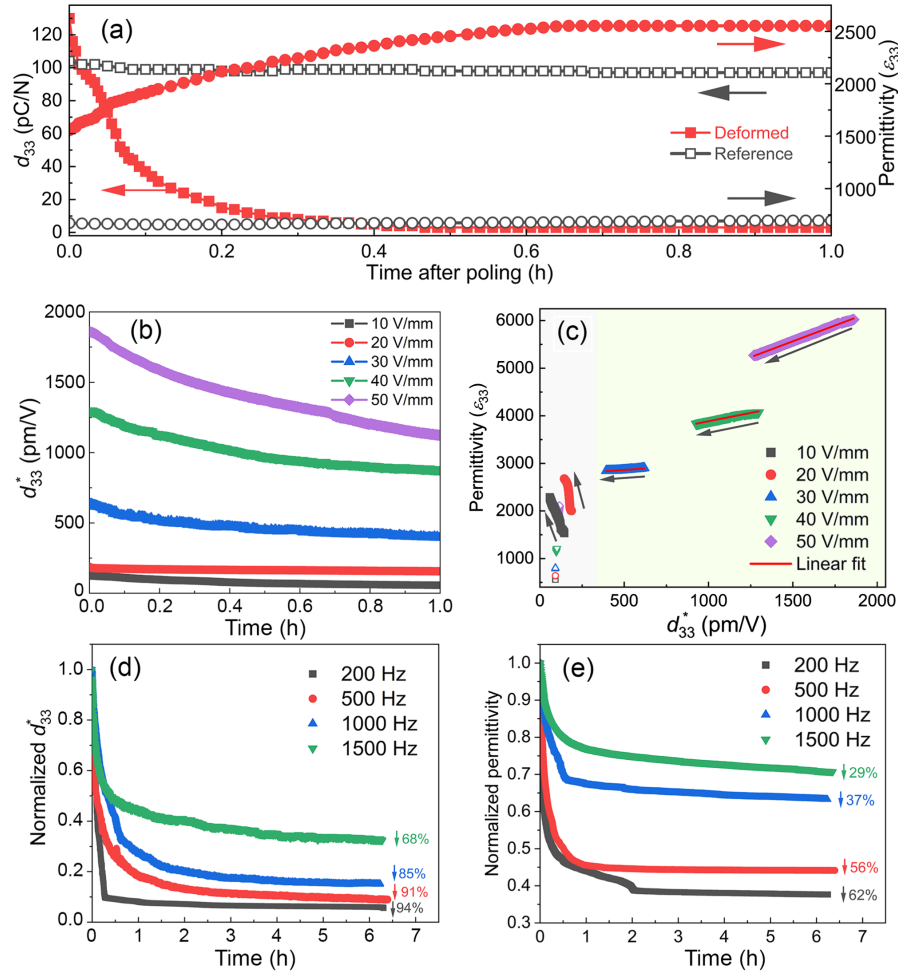
FIG. 3.   (a) Measured d_{33} and ε_{33} as a function of time during the aging process after poling. (b) d_{33}^* as a function of cycling time at different amplitudes of ac fields for the deformed sample quantified at room temperature with a frequency of 1 kHz. (c) The relationship between ε_{33} and d_{33}^* at different amplitudes of the ac fields for both reference (open symbols) and deformed (solid symbols) samples, respectively. Note that the arrows indicate the increase in cycling time. Long-term dislocation-induced fatigue stability of (d) d_{33}^* and (e) ε_{33} under an ac field of 50 V/mm at different frequencies.

switching from c/a domains to a_1/a_2-domain structures, which can be rationalized due to the anisotropy of the dielectric tensor of BaTiO$_3$ with $\varepsilon_a > \varepsilon_c$ [39] and driving force for the motion of DWs, see detailed discussion in Fig. S12 [31]. The observed domain switching by optical microscopy is in good agreement with our phase-field simulations (see Fig. S13 [31]). Our results suggest that dislocations can largely affect the domain switching behavior during aging process. Second, fatigue experiments highlight that the above-mentioned crystallographic anisotropy still plays a dominant role in piezoelectric degradation and the dielectric enhancement at low alternating current (ac) fields (<30 V/mm), see converse piezoelectric coefficient (d_{33}^*) in Fig. 3(b) and d_{33}^* vs ε_{33} in Fig. 3(c). A strong degradation in d_{33}^* was observed when the applied ac fields were higher than 30 V/mm [Fig. 3(b)]. Interestingly, under the same ac field, both d_{33}^* and ε_{33} decreased with a linear relationship during fatigue process

[Fig. 3(c)], insinuating that dislocation-induced effects are dominant. Changing the frequency of the applied ac field of 50 V/mm highlights the significant impact of ⟨100⟩-type dislocations on the dielectric and piezoelectric response. As displayed in Fig. 3(d), the degradation or fatigue in d_{33}^* was alleviated by increasing the frequency from 200 to 1500 Hz (degradation reduced from 94% to 68%). To gain microstructural insight into the mechanisms driving the observed degradation in d_{33}^*, we performed *in situ* optical microscopy measurements on the evolution of 90° DWs (see Figs. S14–S16 [31]). The increase of a domains over c-domains fraction is associated with the observed degradation in d_{33}^* because a_1/a_2 90° DWs do not contribute to the piezoelectric response [47,48]. We note that, however, the percent of degradation in ε_{33} is smaller than that of d_{33}^* [compare Fig. 3(e) with Fig. 3(d)] due to the fact that 180° DWs additionally give rise to a dielectric response [49]. The dislocation-associated degradation in the
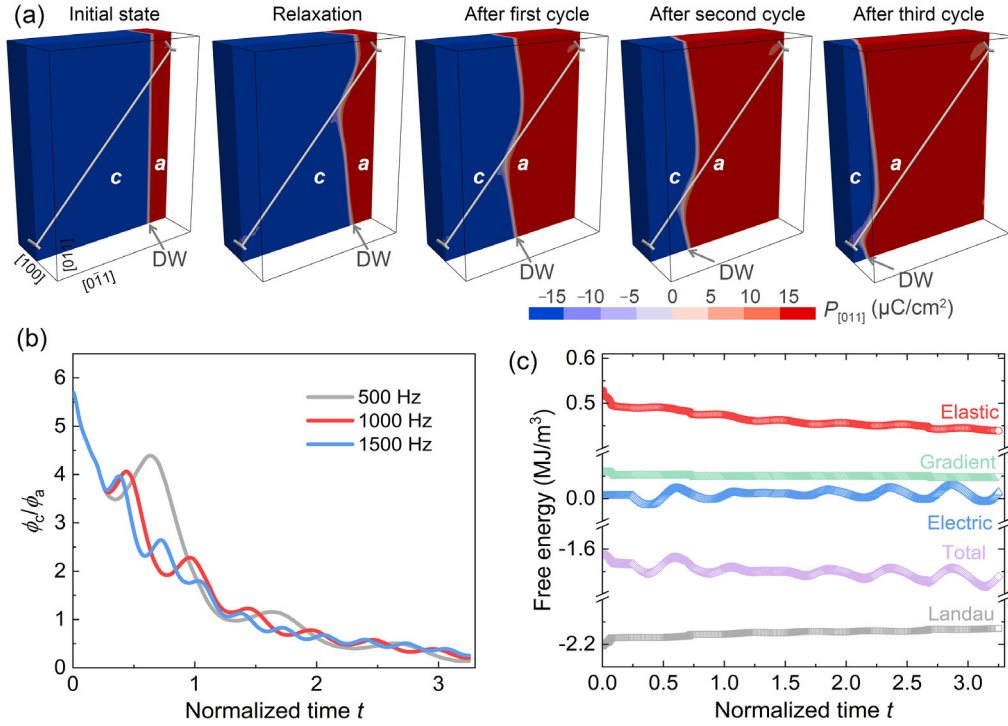
FIG. 4.   (a) Simulated results on the dislocation-induced domain instability with a cycling ac field up to 3 cycles at 500 Hz. The ac field was employed along the [001] direction. (b) Domain fraction as a function of time during the cycling process. The applied field is higher than E_{pin}. (c) Evolution of the simulated energy components as a function of normalized time. The field is higher than E_{pin} with a frequency of 1 kHz. The time is normalized with $T_0 = 0.02$ s.

subcoercive-signal permittivity [Figs. 3(c) and 3(e)] is due to the enhanced domain-wall stiffness and reduced mobility that suppressed the extrinsic contribution (see Sec. 5 in Ref. [31]).

To understand the nature of dislocation-type lattice strains as local drivers initiating the degradation of both d_{33}^* and ε_{33}, we employed phase-field simulations [22,24,32,50] to probe the evolution of domains and free energies during the ac cycling process. As featured in Fig. 4(a), the a/c 90° domain wall bows out towards the tensile side of the dislocation after relaxation. The driving force provided by dislocations initiates the movement of the domain wall on the tensile side of the dislocation and drives the wall on the compressive side to move. The relative population of the c-/a domains was calculated by

$$\phi_c/\phi_a = \left(1 + \frac{\langle P_{[011]}\rangle}{V P_{[011]}^S}\right) \bigg/ \left(1 - \frac{\langle P_{[011]}\rangle}{V P_{[011]}^S}\right), \qquad (1)$$

where $\langle P_{[011]}\rangle = (1/V)\int_V P_{[011]}dV$ is the volume average of the polarization, V is the volume of the system, and $P_{[011]}^S$ is the spontaneous polarization in the [011] direction, respectively. The motion of the domain wall can be stopped by a critical pinning electric field (E_{pin}) [51]. When the ac field is larger than E_{pin}, a wavelike instability of the c/a ratio evolves in a similar fashion at different frequencies

[see Fig. 4(b) as well as detailed interactions in supplemental video S2 [31]]. Specifically, we have monitored the evolution of Landau free energy (charge d.o.f.), elastic energy (lattice d.o.f.), electric (electrostatic) energy (charge d.o.f.), and gradient energy (also charge d.o.f.) during the cycling process. We note that this wavelike c/a ratio instability is almost entirely determined by a reduction in the elastic energy and an increment of the Landau and electric energies, as highlighted in Fig. 4(c) for the case at 1 kHz. This competition between elastic, Landau and electric energies effectively launches the oscillatory nature of the total energy and a corresponding reduction of polarization in the out-of-plane direction that drives the formation of the in-plane a domains (that is, the reduction of c/a ratio). Therefore, the degradation of d_{33}^* is expected, supporting our observation in Fig. 3(b). Increasing the frequency marks the evolution of various energies in the same manner (see simulated results at 500 and 1500 Hz in Fig. S17 [31]). A lower frequency has a stronger influence on the movement of the wall, resulting in a smaller volume fraction of c domains after cycling for the same time interval [Fig. 4(b)], which rationalizes the experimental observations in Fig. 3(d). Our case of well-aligned dislocation imprint allows us to substantially modify the relative fraction of domains, the evolution of lattice and charge degrees of freedom, and related properties of ferroelectrics by simple aging and fatigue experiments.

In summary, we demonstrated the intrinsic ability to control the nucleation and stability of in-plane domains in a prototype ferroelectric BaTiO$_3$ single crystal by mechanically introducing well-selected dislocation-structures. Hence, we provide a means to tune domain structure, dielectric and piezoelectric properties of a bulk sample by plastic deformation that radically changed the lattice degree of freedom, overcoming the substrate limitation of elastic strain engineering. Beyond the long-recognized effects of dislocations on domain nucleation and domain-wall pinning in ferroelectrics, we revealed the role of dislocations on domain switching during both aging and fatigue. Dislocations initiated the degradation sites for the dielectric and electromechanical response, opening a pathway to understand the structure-property relationships of defect sites, and hence the optimization and control of these processes. Our result delivers a tool for the demonstration of domain control using structural defects, such as out-of-phase boundaries [52,53].

---

[*]These two authors contributed equally to this work.
[†]zhuo@ceramics.tu-darmstadt.de
[‡]roedel@ceramics.tu-darmstadt.de

[1] D. G. Schlom, L. Q. Chen, C. B. Eom, K. M. Rabe, S. K. Streiffer, and J. M. Triscone, Annu. Rev. Mater. Res. **37**, 589 (2007).

[2] I. Bozovic, G. Logvenov, I. Belca, B. Narimbetov, and I. Sveklo, Phys. Rev. Lett. **89**, 107001 (2002).

[3] C. Ederer and N. A. Spaldin, Phys. Rev. Lett. **95**, 257601 (2005).

[4] J. H. Haeni, P. Irvin, W. Chang, R. Uecker, P. Reiche, Y. L. Li, S. Choudhury, W. Tian, M. E. Hawley, B. Craigo, A. K. Tagantsev, X. Q. Pan, S. K. Streiffer, L. Q. Chen, S. W. Kirchoefer, J. Levy, and D. G. Schlom, Nature (London) **430**, 758 (2004).

[5] D. Damjanovic, Rep. Prog. Phys. **61**, 1267 (1998).

[6] V. G. Koukhar, N. A. Pertsev, and R. Waser, Phys. Rev. B **64**, 214103 (2001).

[7] N. A. Pertsev, A. G. Zembilgotov, and A. K. Tagantsev, Phys. Rev. Lett. **80**, 1988 (1998).

[8] K. J. Choi, M. Biegalski, Y. L. Li, A. Sharan, J. Schubert, R. Uecker, P. Reiche, Y. B. Chen, X. Q. Pan, V. Gopalan, L. Q. Chen, D. G. Schlom, and C. B. Eom, Science **306**, 1005 (2004).

[9] A. Gruverman, D. Wu, H. Lu, Y. Wang, H. W. Jang, C. M. Folkman, M. Ye. Zhuravlev, D. Felker, M. Rzchowski, C.-B. Eom, and E. Y. Tsymbal, Nano Lett. **9**, 3539 (2019).

[10] A. R. Damodaran, S. Pandya, J. C. Agar, Y. Cao, R. K. Vasudevan, R. Xu, S. Saremi, Q. Li, J. Kim, M. R. McCarter, L. R. Dedon, T. Angsten, N. Balke, S. Jesse, M. Asta, S. V. Kalinin, and L. W. Martin, Adv. Mater. **29**, 1702069 (2017).

[11] J. Karthik, A. R. Damodaran, and L. W. Martin, Phys. Rev. Lett. **108**, 167601 (2012).

[12] H. Fu and R. E. Cohen, Nature (London) **403**, 281 (2000).

[13] G. Catalan, J. Seidel, R. Ramesh, and J. F. Scott, Rev. Mod. Phys. **84**, 119 (2012).

[14] L. Zhang, J. Chen, L. Fan, O. Diéguez, J. Cao, Z. Pan, Y. Wang, J. Wang, M. Kim, S. Deng, J. Wang, H. Wang, J. Deng, R. Yu, J. F. Scott, and X. Xing, Science **361**, 494 (2018).

[15] M. Dawber, K. M. Rabe, and J. F. Scott, Rev. Mod. Phys. **77**, 1083 (2005).

[16] L. W. Martin, Y. H. Chu, and R. Ramesh, Mater. Sci. Eng. R **68**, 89 (2010).

[17] X. Ren, Nat. Mater. **3**, 91 (2004).

[18] Y.-H. Shin, I. Grinberg, I-W. Chen, and A. M. Rappe, Nature (London) **449**, 881 (2007).

[19] R. Ignatans, D. Damjanovic, and V. Tileli, Phys. Rev. Lett. **127**, 167601 (2021).

[20] N. Doukhan and J. C. Doukhan, Phys. Chem. Miner. **13**, 403 (1986).

[21] S. Beauchesne and J. P. Poirier, Phys. Earth Planet. Inter. **55**, 187 (1989).

[22] M. Höfling, X. Zhou, L. M. Riemer, E. Bruder, B. Liu, L. Zhou, P. B. Groszewicz, F. Zhuo, B.-X. Xu, K. Durst, X. Tan, D. Damjanovic, J. Koruza, and J. Rödel, Science **372**, 961 (2021).

[23] D. Hull and D. J. Bacon, *Introduction to Dislocations* (Elsevier, Oxford, 2011).

[24] S. Y. Hu, Y. L. Li, and L. Q. Chen, J. Appl. Phys. **94**, 2542 (2003).

[25] H. H. Wu, J. Wang, S. G. Cao, and T. Y. Zhang, Appl. Phys. Lett. **102**, 232904 (2013).

[26] A. Kontsos and C. M. Landis, Int. J. Solids Struct. **46**, 1491 (2009).

[27] P. Gumbsch, S. Taeri-Baghbadrani, D. Brunner, W. Sigle, and M. Ruhle, Phys. Rev. Lett. **87**, 085505 (2001).

[28] L. B. Freund and S. Suresh, *Thin Film Materials: Stress, Defect Formation and Surface Evolution* (Cambridge University Press, Cambridge, England, 2004).

[29] M. Höfling, L. Porz, M. Scherer, S. Gao, F. Zhuo, D. Isaia, and J. Rödel, J. Mater. Res. **37**, 737 (2022), https://link.springer.com/article/10.1557/s43578-022-00485-6.

[30] L. W. Martin and A. M. Rappe, Nat. Rev. Mater. **2,** 1 (2016).

[31] See Supplemental Material at http://link.aps.org/supplemental/10.1103/PhysRevLett.131.016801 for additional information on methods, optical images, and PFM data; temperature-dependent small-signal permittivity and polarization hysteresis loops; aging on deformed samples after [110] poling; videos; phase-field simulation results; and details of the phase-field model. There the additional Refs. [32–38] involved.

[32] X. Zhou, Z. Liu, and B.-X. Xu, Int. J. Solids Struct. **238,** 111391 (2022).

[33] Y. L. Li, S. Y. Hu, S. Choudhury, M. I. Baskes, A. Saxena, T. Lookman, Q. X. Jia, D. G. Schlom, and L. Q. Chen, J. Appl. Phys. **104,** 104110 (2008).

[34] W. Cai, A. Arsenlis, C. R. Weinberger, and V. V. Bulatov, J. Mech. Phys. Solids **54,** 561 (2006).

[35] C. J. Permann, D. R. Gaston, D. Andrš, R. W. Carlsen, F. Kong, A. D. Lindsay, J. M. Miller, J. W. Peterson, A. E. Slaughter, R. H. Stogner, and R. C. Martineau, SoftwareX **11,** 100430 (2020).

[36] Y. Su and C. M. Landis, J. Mech. Phys. Solids **55,** 280 (2007).

[37] G. Arlt and N. A. Pertsev, J. Appl. Phys. **70,** 2283 (1991).

[38] N. A. Pertsev, G. Arlt, and A. G. Zembilgotov, Phys. Rev. Lett. **76,** 1364 (1996).

[39] W. J. Merz, Phys. Rev. **95,** 690 (1954).

[40] J. Nordlander, F. Eltes, M. Reynaud, J. Nürnberg, G. De Luca, D. Caimi, A. A. Demkov, S. Abel, M. Fiebig, J. Fompeyrine, and M. Trassin, Phys. Rev. Mater. **4,** 034406 (2020).

[41] F. Zhuo, X. Zhou, S. Gao, M. Höfling, F. Dietrich, P. B. Groszewicz, L. Fulanović, P. Breckner, A. Wohninsland, B.-X. Xu, H.-J. Kleebe, X. Tan, J. Koruza, D. Damjanovic, and J. Rödel, Nat. Commun. **13,** 6676 (2022).

[42] U. Messerschmidt, *Dislocation Dynamics During Plastic Deformation* (Springer, Berlin, Heidelberg, 2010).

[43] O. Liechti and R. Kind, J. Magn. Reson. **85,** 480 (1989).

[44] S. P. Alpay, I. B. Misirlioglu, V. Nagarajan, and R. Ramesh, Appl. Phys. Lett. **85,** 2044 (2004).

[45] P. Gao, C. T. Nelson, J. R. Jokisaari, S. H. Baek, C. W. Bark, Y. Zhang, E. Wang, D. G. Schlom, C. B. Eom, and X. Pan, Nat. Commun. **2,** 591 (2011).

[46] I. Vrejoiu, G. L. Rhun, N. D. Zakharov, D. Hesse, L. Pintilie, and M. Alexe, Philos. Mag. **86,** 4477 (2006).

[47] F. Xu, S. Trolier-McKinstry, W. Ren, B. Xu, Z.-L. Xie, and K. J. Hemker, J. Appl. Phys. **89,** 1336 (2001).

[48] N. Bassiri-Gharb, I. Fujii, E. Hong, S. Trolier-McKinstry, D. V. Taylor, and D. Damjanovic, J. Electroceram. **330,** 47 (2007).

[49] C. M. Fancher, S. Brewer, C. C. Chung, S. Röhrig, T. Rojac, G. Esteves, M. Deluca, N. Bassiri-Gharb, and J. L. Jones, Acta Mater. **126,** 36 (2017).

[50] X. Zhou, C. Reimuth, P. Stein, and B.-X. Xu, Arch. Appl. Mech. **91,** 4499 (2021).

[51] M. Peach and J. S. Koehler, Phys. Rev. **80,** 436 (1950).

[52] E. Gradauskaite, K. A. Hunnestad, Q. N. Meier, D. Meier, and M. Trassin, Chem. Mater. **34,** 14, 6468 (2022).

[53] H. Nakajima, K. Kurushima, S. Mine, H. Tsukasaki, M. Matsuoka, B. Gao, S.-W. Cheong, and S. Mori, Comm. Mater. **2,** 109 (2021).